PERGAMON

International Journal of Heat and Mass Transfer 41 (1998) 3515–3528

International Journal of HEAT and MASS TRANSFER

The effect of injection hole length on film cooling with bulk flow pulsations

H. J. Seo[a], J. S. Lee[a,*], P. M. Ligrani[b]

[a] *Turbo and Power Machinery Research Center, Department of Mechanical Engineering, Seoul National University, Seoul 151-742, Korea*

[b] *Convective Heat Transfer Laboratory, Department of Mechanical Engineering, University of Utah, Salt Lake City, UT 84112, U.S.A.*

Received 30 July 1997; in final form 9 January 1998

Abstract

Bulk flow pulsations in the form of sinusoidal variations of velocity and static pressure at injectant Strouhal numbers from 0.1–10.1 are investigated as they affect film cooling from a single row of simple angle holes. Similar flow variations are produced by potential flow interactions and passing shock waves near turbine surfaces in gas turbine engines. Time-averaged temperature distributions, phase-averaged temperature distributions, adiabatic film cooling effectiveness values, and iso-energetic Stanton numbers show that important alterations to film cooling protection occur at different ranges of frequencies and coolant Strouhal numbers as non-dimensional injection hole length is changed.

Nomenclature

D injection hole diameter
f pulsation frequency
H boundary layer shape factor
L injection hole length
$\bar{m}$ time-averaged blowing ratio, $\bar{m} = \rho_c \bar{U}_c / \rho_\infty \bar{U}_\infty$
M_c coolant flow Mach number
$\tilde{p}_0$ phase-averaged static pressure at the plenum chamber
$\tilde{p}_\infty$ phase-averaged free-stream static pressure
$\dot{q}''_0$ surface heat flux with no film cooling
$\dot{q}''$ spanwise-averaged surface heat flux with film cooling
Re_c coolant Reynolds number, $Re_c = \bar{U}_c D/\nu$
Re_x free-stream Reynolds number, $Re_x = \bar{U}_\infty X/\nu$
Str_c injectant Strouhal number, $Str_c = 2\pi f L/\bar{U}_c$
Str_∞ free-stream Strouhal number, $Str_\infty = 2\pi f \delta/\bar{U}_\infty$
$St_{f,c}$ centerline iso-energetic Stanton number
$St_{f,m}$ spanwise-averaged iso-energetic Stanton number
St_0 baseline Stanton number with no pulsations and no film cooling
T instantaneous temperature
$\bar{T}$ time-averaged temperature
$\tilde{T}$ phase-averaged temperature
$\tilde{T}'$ phase-averaged component, $\tilde{T}' = \tilde{T} - \bar{T}$
T' temperature fluctuation
T_{aw} adiabatic wall temperature
T_c injectant temperature at exit planes of film holes
T_∞ free-stream temperature
$\bar{U}_c$ time-averaged injectant velocity
$\bar{U}_\infty$ time-averaged free-stream velocity
$\tilde{U}_\infty$ phase-averaged free-stream velocity
x, X, y, z coordinate system.

Greek symbols
δ boundary layer thickness
δ^* boundary layer displacement thickness
η local film cooling effectiveness, $\eta = (T_{aw} - T_\infty)/(T_c - T_\infty)$
η_m spanwise-averaged film cooling effectiveness, $\eta_m = (T_{aw,m} - T_\infty)/(T_c - T_\infty)$
θ boundary layer momentum thickness
Θ dimensionless temperature, $\Theta = (\bar{T} - T_\infty)/(T_c - T_\infty)$
ν kinematic viscosity
τ pulsation period.

* Corresponding author. Tel.: 00-82-2-880-7117; fax:00-82-2-883-0179; e-mail: jslee@gong.snu.ac.kr.

0017–9310/98 $19.00
PII: S0017–9310(98)00042–8

Superscripts
$\bar{}$ time-averaged
$\tilde{}$ phase-averaged
$'$ fluctuating component.

Subscripts
c injectant
m spanwise-averaged
∞ free-stream.

1. Introduction

Film cooling is widely used to cool and thereby protect, turbine component surfaces from exposure to the hot gases produced in combustion chambers of high performance gas turbine engines. These film cooling flows operate in flows which are inherently unsteady because of the relative motion of adjacent blade rows. In transonic turbine passages, this unsteadiness is due to: (i) passing families of shock waves, (ii) potential flow interactions, (iii) passing wakes, and (iv) random (and sometimes periodic) free-stream turbulence from the combustion chamber. Of these different modes of unsteadiness, a number of recent investigations document the dramatic effects of potential flow interactions and passing shock waves in altering the protection nominally provided by film cooling [1–6]. Both of these modes of unsteadiness result in important variations of the static pressure near turbine airfoil surfaces as blade rows move relative to each other. As a result, film concentrations and film trajectories move to and from the wall with each imposed bulk flow pulsation because of instantaneous changes to the film flow rate and momentum at the cooling hole exits, and then act to alter the time-averaged position of the film and mean-injectant trajectory as the pulsations act to spread the same amount of injectant over a larger volume [2]. According to Ligrani et al. [3, 5, 6], such important changes to time-averaged film cooling protection and flow structure have important consequences regarding design of film cooling systems for turbine surfaces.

In an investigation of rotor heat transfer in a short-duration blow-down turbine test facility, Abhari and Epstein [1] indicate that flow pulsations cause the time-averaged heat transfer rate to increase by 12% on the suction surface and to decrease by 5% on the pressure surface compared with values measured with no pulsations; two rows of holes are employed on the suction surface of the rotor blade with blowing ratios from 0.96–1.24, and three rows of holes are employed on the pressure surface with blowing ratios from 1.1–1.52. Abhari [4] later predicted time-averaged magnitudes of unsteady surface heat flux on the pressure surface of a similarly cooled rotor blade which are 230% greater than steady-state predictions; it is attributed to reductions of adiabatic film effectiveness by as much as 64%, and according to the author, unsteady pressure fluctuations can either increase or decrease the time-averaged coolant fluxes downstream of the film cooling holes, depending upon the details of the film hole design, hole placement, and turbine operating conditions.

A number of experiments described by Ligrani et al. [2, 3, 5, 6] are conducted on a large scale with low speeds, flat plate test sections, and constant property flows to allow detailed probing of flow features, and to isolate the interactions between the film, the imposed bulk flow pulsations, and the boundary layer. Pulsation frequencies range of 0.2–8 Hz, which correspond to the injectant Strouhal numbers from 0.36–8.12 at blowing ratios from 0.1–2.0. The L/D ratio of the holes is 4.0. Flow visualization results [2] evidence two distinct injectant flow regimes: quasi-steady and non-quasi-steady. For the single L/D ratio employed in the study, magnitudes of injectant Strouhal number, Str_c, less than $1 \sim 2$ correspond to quasi-steady behavior, and magnitudes greater than $1 \sim 2$ correspond to non-quasi-steady behavior, regardless of the magnitude of the blowing ratio. Quasi-steady film distributions are the same as the steady distribution which would exist at the same instantaneous flow condition. With non-quasi-steady film behavior, multiple pulsations are imposed on the injectant over the time period required for it to pass through a film hole. As a result, portions of the film oscillate in ways different from adjacent portions, which gives a 'wavy' appearance (when viewed from the side) at each instant in time [2]. In many cases, non-quasi-steady film distributions lead to more important alterations to film effectiveness magnitudes and flow structure than when quasi-steady behavior is present [3, 5, 6].

The present study employs different experimental conditions than those investigated by Ligrani et al. [2, 3, 5, 6]. Different amplitudes of pulsations are used here, and a larger range and higher values of pulsation frequencies (2, 16, and 32 Hz) are employed. In addition, no trips are used near the entrances to the film holes as they were in the earlier investigations [2, 3, 5, 6]. Here, the blowing ratio is also fixed at 0.5. Because of its importance to film cooling system design, film cooling performance and behavior downstream of holes with three different L/D values of 1.6, 4.0 and 10 are investigated. The results, for the experimental conditions where important disruptions to film protection occur, show complex dependence upon the magnitudes of the injectant Strouhal number and L/D. A single limiting value of injectant Strouhal number Str_c will not be sufficient by itself to characterize the experimental conditions where important film effectiveness decreases occur as L/D and Str_c are varied.

2. Experimental apparatus and measurements

As in recent previous investigations [2, 3, 5, 6], the present experiment is conducted on a large scale with a

flat plate test section, low speeds, and constant properties, to allow detailed probing of flow features, and to isolate the interactions between the film cooling, imposed pulsations, and boundary layer. Important parameters are scaled so that non-dimensional forms match transonic turbine operating conditions.

The wind tunnel is an open-circuit and subsonic, with a 6.25 : 1 contraction ratio nozzle. The nozzle leads to the test section which is a rectangular duct 3.0 m long and 0.4 m wide. For free-stream velocity of 10 m s^{-1}, flow at the test section inlet shows excellent spatial uniformity, with freestream streamwise velocity variations less than 0.5%, and a free-stream turbulence level less than 0.2%. A schematic of the test section, including the coordinate system and injection hole arrangement, is shown in Fig. 1. A boundary layer trip is located on the test plate just downstream of the nozzle exit. The center of the injection holes is located 24 hole diameters downstream of the trip. Hole diameter D is 25 mm. The five film cooling holes are placed in a single row with spanwise spacing of 3 hole diameters. Each hole is oriented in a streamwise/normal plane (i.e. with a simple angle orientation) inclined at a 35° angle from the test surface. The air used for the injectant first flows through an orifice followed by a heat exchanger and a plenum chamber. Pressure drops across the orifice plate are measured to deduce injectant mass flow rates. The heat exchanger heats the injectant above ambient temperature. The interior dimensions of the plenum chamber, for supplying injectant to the film holes, are 0.58 m × 0.48 m × 0.48 m. Film hole entrances are located on the side of the plenum with the largest surface area, located on the top.

Experimental conditions are summarized in Table 1. The free-stream mean velocity is fixed at 10 m s^{-1} and the Reynolds number, $\bar{U}_\infty X/\nu$, at the hole center is 614 000, where X is measured from the leading edge of the trip. Ratios of boundary layer thickness to hole diameter (δ^*/D), displacement thickness to hole diameter (δ/D), and momentum thickness to hole diameter (θ/D) at the same location are 1.02, 0.12 and 0.08, respectively. Time-averaged blowing ratio $\bar{m}$ is 0.5. The ratio of injectant to

Table 1
Experimental conditions

$\bar{U}_\infty$	10 m s^{-1}
D	25 mm
Re_x	614 000
δ/D	1.02
δ^*/D	0.12
θ/D	0.08
H	1.43
$\bar{m}$	0.5
L/D	1.6, 4, 10
f	0, 2, 16, 32 Hz

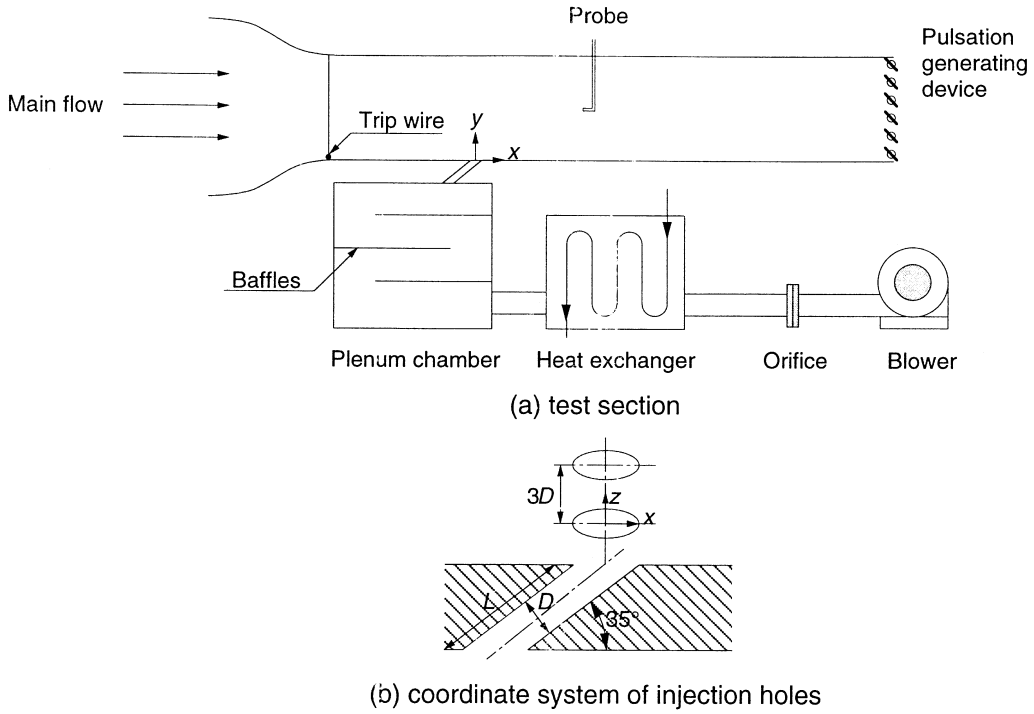

Fig. 1. Schematic drawing of test section and coordinate system.

free-stream density is approximately 0.93 for the injectant surveys. The injectant Reynolds number, $Re_c = \bar{U}_c D/\nu$, is 7800. Injectant and free-stream Strouhal numbers are listed in Table 2. Ratios of injection hole length to hole diameter, L/D, are 1.6, 4.0 and 10. Pulsation frequency ranges from 0–32 Hz. Corresponding injectant and free-stream Strouhal numbers range from 0.1–10.1, and from 0.032–0.51, respectively.

A 5 μm diameter hot-wire probe, driven by a constant temperature hot-wire anemometer (CTA) system, is used to measure free-stream velocity pulsations. Static pressure pulsations at the plenum chamber and at the exit of the injection hole are measured using a piezo-resistive pressure sensor with 1 kHz frequency response. The temperatures, which are correlated to injection distributions, are measured using a 1 μm diameter cold-wire probe driven by a constant current anemometer. The frequency response of the electronic components of this constant current system is 1 kHz. Steady-state calibration of the cold wire system is performed using a platinum resistance thermometer (with a relative error of 0.1%) as a reference. Time-averaged quantities are obtained using a multimeter with a resolution of 10 nV which corresponds to a measurement error of $\pm 0.05^{\circ}$C. Time varying quantities are recorded using a digital data acquisition system, which includes a multiplexer and an analog-to-digital converter. Phase-averaged quantities are deduced from these data time records using procedures described below.

With imposed periodic flow, the instantaneous temperature T is decomposed using an equation of the form

$$T = \bar{T} + \tilde{T}' + T' = \tilde{T} + T' \quad (1)$$

where $\bar{T}$ is the time-averaged temperature $\tilde{T}$ is the phase-averaged temperature, and T' is the fluctuating component. The time period used in the determination of phase-averaged values is based on the angular speed of the encoder of the motor used to drive the rotating shutter blades which are used to pulsate the flow. One motor rotation corresponds to two flow pulsation periods. Signals from more than 500 flow pulsations periods are ensemble averaged to obtain each phase-average. Data are sampled digitally to obtain 1000 data points over each flow pulsation period. Individual phase-averaged wave forms are determined at 100 equally spaced times through each flow pulsation period.

Table 2
Strouhal numbers

f [Hz]	L/D	Str_c	Str_∞
2	1.6	0.1	0.032
	4	0.25	
	10	0.63	
16	1.6	0.8	0.26
	4	2.01	
	10	5.03	
32	1.6	1.59	0.51
	4	4.02	
	10	10.1	

Adiabatic film cooling effectiveness distributions are determined from measurements of the freestream temperature, the injectant temperature, and distributions of the surface temperature, measured using 96 T-type thermocouples installed along the test surface. Next to the air stream, this test surface is 25 μm thick stainless steel foil. A 12.7 mm thick Lexan plate is attached just beneath the foil. Beneath this, 50 mm of styrofoam is used as an insulator. Temperature differences between the lower and upper surfaces of the Lexan are generally less than 5% of the temperature difference between the injectant and free-stream. Injectant temperatures are measured in the injectant plenum chamber near the inlet of one of the injection tubes. Each of these tubes is well insulated to minimize heat transfer to or from the injectant, and to minimize temperature changes between the entrance and exit of each tube.

Iso-energetic Stanton numbers are measured when the test surface is heated. The same test surface used to obtain the adiabatic effectiveness measurements is employed and thus, the same 96 thermocouples measure surface temperatures used to compute surface heat transfer coefficients and Stanton numbers. A constant heat flux boundary condition is provided by passing current through the 25 μm thick stainless steel foil located next to the air stream. Injectant and freestream temperatures are the same to maintain an iso-energetic condition. Radiation losses are determined analytically. Energy balances, used to estimate the amount of convection from the test plate to the air stream above, show that conduction losses from beneath the test surface are negligible compared to power supplied to the foil heater.

Uncertainty estimates are determined based on 95% confidence level using the method described by Kline and McClintock [7]. The uncertainty in the dimensionless temperature Θ is 5.0% and the uncertainty of the local film cooling effectiveness η is 7.1%. The uncertainty of the iso-energetic heat transfer coefficient (used to determine the iso-energetic Stanton number, St) is 3.9%.

3. Generation and characteristics of flow pulsations

Static pressure pulsations are produced by an array of six shutter blades, which are driven by a DC motor and a timing belt, and extend across the span of the exit of the wind tunnel test section. Periodic blockage is produced by the shutter blades as they rotate. Their sizes relative to the cross sectional area of the test section exit set the

amplitudes of the imposed flow pulsations. Each shutter has 25.0 mm width (which gives maximum blockage) when perpendicular to the flow, and 1.5 mm thickness (for minimum blockage) across the 0.28 m high by 0.4 m wide exit area. This gives a ratio of maximum blockage area to the total open test section area of 0.53, instead of 0.73 in the investigations [2, 3, 5, 6].

Freestream pulsation amplitudes in the present study, $(\tilde{U}_{\infty,\max}-\tilde{U}_{\infty,\min})/2\bar{U}_{\infty}$, are about 18.2% at 2 Hz and decrease to 5.7 and 4.4% as the pulsation frequency increases to 16 and 32 Hz, respectively. The pulsation amplitudes produced by Ligrani et al. [6] at the same freestream velocity (10 m s^{-1}) are about 20.1% at 2 Hz. Thus, the pulsation amplitudes produced by the present device are about the same, as reported in [2, 3, 5, 6].

Rotating vanes are employed to provide flow pulsations owing to the considerations: (i) the shutters oscillate the static pressure without significant total pressure variations [8, 9], (ii) static pressure pulsations produce the most important disruptions to the flow rates, trajectories, and distributions of the film coolant, (iii) much higher frequencies of pulsation can be produced [8], and (iv) deterministic sinusoidal variations of static pressure can be produced at selected frequencies [9]. The sinusoidal characteristics of the phase-averaged free-stream velocity $\tilde{U}_{\infty}$ wave forms produced by the pulsation device are illustrated in Fig. 2. Similar wave form at 2 Hz was described by Ligrani et al. [6]. Spectra of longitudinal velocity fluctuations, also from that study [6], show a large local maximum at the frequency of the principal oscillation with amplitudes at harmonic frequencies which are at least two orders of magnitude lower in amplitude.

A number of different time scales affect the behavior of film cooled boundary layers subject to bulk flow pulsations. The response time of a boundary layer subject to periodic disturbances is characterized by free-stream Strouhal number $Str_{\infty}=2\pi f\delta/\bar{U}_{\infty}$ [9]. According to Abhari and Epstein [1], adjustment of coolant flow rates

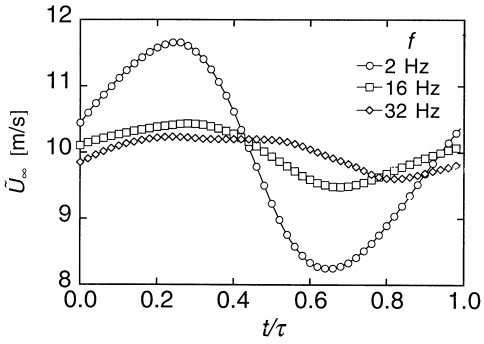

Fig. 2. Typical free-stream velocity wave forms at different pulsation frequencies.

is characterized by the product of coolant flow Mach number M_c and coolant Strouhal number $Str_c=2\pi fL/\bar{U}_c$. Temporal pressure variations will influence the coolant mass flow rate when the disturbance frequency is low compared with the time required for the flow to pass through the coolant holes. This occurs if the product of coolant flow Mach number M_c and coolant Strouhal number is about 1 or less ($M_c\ Str_c \leqslant 1$) [1]. Typical values for operating turbines range from 0.2–0.6, which gives Str_c from 0.2–6.0. In the present experiment, Str_c ranges from 0.1–10.1.

4. Results and discussion

4.1. Bulk flow pulsation characteristics

The phase-averaged free stream velocity, traced in Fig. 2, illustrates that wave form characteristics at 16 Hz and 32 Hz are different from the wave form at 2 Hz. Lower amplitudes result at higher imposed pulsation frequencies due to flow inertia which causes timewise variations of the streamwise velocity to lag behind the static pressure pulsations imposed at the test section outlet. It is evident in Fig. 2, that the non-sinusoidal behavior of the free-stream velocity wave form at 32 Hz. According to Al-Asmi and Castro [8], the shapes of freestream pulsation wave forms are affected by the resonance frequency of the wind tunnel. Wave forms are more likely to be sinusoidal in shape when the pulsation frequency is a multiple of the resonance frequency of the wind tunnel, and less likely to be sinusoidal at other frequencies. The resonance frequency of a wind tunnel depends upon the length of the flow passage, turbulence generating grids, honey combs/screens, and diverging or converging sections. The present wind tunnel resonance frequency is estimated to be about 12 Hz, which is consistent with the results in Fig. 2.

Differences between the phase-averaged plenum chamber pressure, $\tilde{p}_0$, and the phase-averaged freestream pressure, $\tilde{p}_{\infty}$, at different pulsation frequencies and different L/D are shown in Fig. 3. Here, p_0 is measured on the top wall of the plenum chamber 104 mm (or 4.16D) from the center of the film hole which is located at $z/D=-6$, while p_{∞} is measured on the bottom wind tunnel test surface near the exits of the film cooling holes. Smaller variations of $(\tilde{p}_0-\tilde{p}_{\infty})$ were reported in Refs. [2, 3, 5, 6] studies because of their larger film injection plenum. Largest changes occur as the pulsation frequency is changed as L/D is held constant. The larger amplitude $(\tilde{p}_0-\tilde{p}_{\infty})$ wave forms at 32 Hz as compared to 16 Hz and 2 Hz are mostly due to larger phase shifts between instantaneous p_0 and p_{∞} at larger pulsation frequencies. Thus, the $(\tilde{p}_0-\tilde{p}_{\infty})$ variations are affected by time-wise variations of both the freestream static pressure as well as the pressure in the injection plenum. The magnitudes

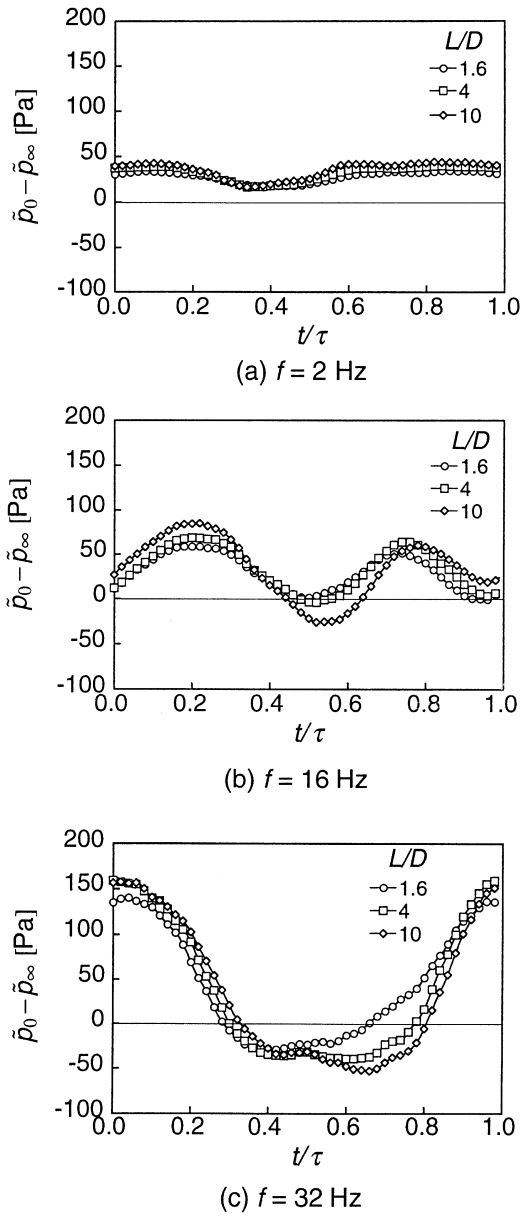

Fig. 3. Variation of difference between the static pressure in the plenum and static pressure in the freestream with pulsation frequency, L/D and the time instant (t) relative to pulsation period (τ).

of the pressure variations in the plenum chamber decrease as the pulsation frequency increases. Variations for $f = 16$ Hz and $f = 32$ Hz are quite small, generally less than 10–15% of time-averaged values.

Phase shifts between p_0 and p_∞ are directly connected to the variation of $\tilde{p}_0-\tilde{p}_\infty$ with time, and also, according to Ligrani et al. [2], to the variation of the injectant flow rate with time. The $(\tilde{p}_0-\tilde{p}_\infty)$ variations with time, shown in Fig. 3, are evidently affected by the film flow rate, the pulsation frequency, the injectant plenum size and design, and L/D. The variations which occur in Fig. 3 as L/D is changed at each pulsation frequency, are quantitatively less significant, appearing as changes in wave form shapes, particularly where $(\tilde{p}_0-\tilde{p}_\infty)$ increases with t/τ.

The time-averaged blowing ratio $\bar{m}$ for all of the data in Fig. 3 is 0.50. This corresponds to $\bar{p}_0-\bar{p}_\infty$ (or $\tilde{p}_0-\tilde{p}_\infty$) of about 36–38 Pa. At $f = 16$ Hz and $f = 32$ Hz, $(\tilde{p}_0-\tilde{p}_\infty)$ becomes locally negative over significant portions of the pulsation periods, which gives reversed flow into the holes. This situation occurs over small portions of phase-averaged pulsation periods when $f = 16$ Hz, but over almost half of phase-averaged pulsation periods when $f = 32$ Hz. Changes with L/D are particularly evident at a pulsation frequency of 32 Hz. Such variations are important because they are tied to changes of the injectant flow rate over one pulsation period, and hence, to timewise alterations of injectant trajectories, coverage, and protection.

4.2. Injectant concentration distributions

Phase-averaged, time-averaged, and steady injectant surveys, measured at $x/D = 5.0$ with flow pulsations imposed at 32 Hz, are presented in Figs. 4, 5, and 6 for L/D of 1.6, 4.0, and 10.0, respectively. Local film cooled boundary layer temperature distributions are expressed in non-dimensional form using Θ. These distributions are obtained using techniques developed by Ligrani et al. [11, 12] in which the injectant is heated as all other components in the wind tunnel test section are maintained at the free-stream temperature, and hence, the injectant is the only source of thermal energy relative to the free-stream. Higher magnitudes of Θ then indicate greater concentration of injectant, and clear indications of the protection (or lack of protection) provided by the injectant. Near wall values of Θ are particularly important because they approach magnitudes of the adiabatic film cooling effectiveness [2, 12].

The results for $f = 32$ Hz show that injectant variations with t/τ through pulsation periods become larger as L/D decreases from 10 to 1.6, and are significantly greater than the quantitative differences $(\tilde{p}_0-\tilde{p}_\infty)$ data in Fig. 3(c). Thus, factors in addition to the p_0-p_∞ pressure difference, such as film behavior in the injectant holes, have important effects on distributions, trajectories, and coverage of the film injectant.

Time-averages of injectant distributions subject to bulk flow pulsations are given for $f = 0$, 2 and 16 Hz, as compared with $f = 32$ Hz, in Fig. 7. Corresponding coolant Strouhal numbers are included in the figure and range from 0–10. These results thus summarize effects of f and L/D on time-averaged injectant distributions at

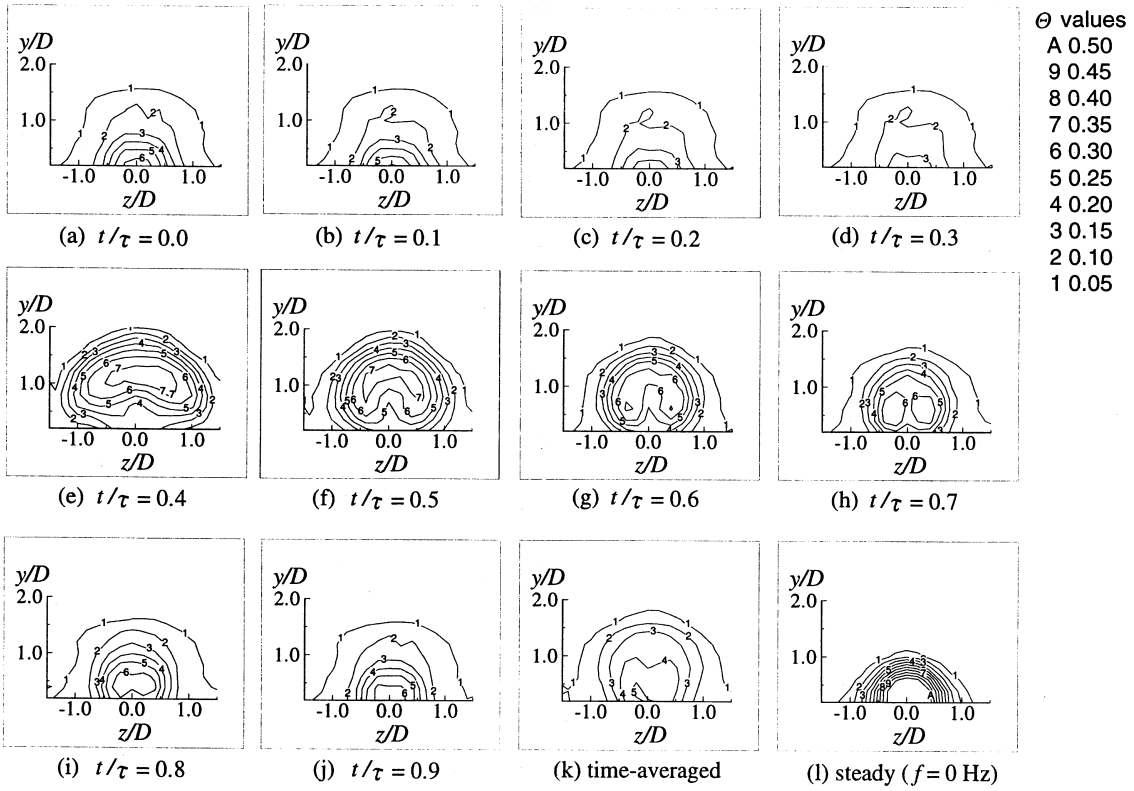

Fig. 4. Phase-averaged injectant concentration Θ distributions at $x/D = 5.0$ for $f = 32$ Hz and $L/D = 1.6$.

$x/D = 5.0$. At each pulsation frequency, Fig. 7 shows that the effects of the pulsations are most significant when $L/D = 1.6$ and weakest for $L/D = 10.0$. Such changes are tied to instantaneous and periodic changes of injectant momentum and injectant trajectory position in the boundary layer, and therefore, to pulsations of the instantaneous injectant flow rate with phase through each pulsation period as being pointed out in Ref. [2]. According to Ligrani et al. [2, 3, 5, 6], alterations to time-averaged injectant distributions and to surface adiabatic effectiveness distributions become larger as pulsation frequency increases.

Injectant distributions in Fig. 7 are consistent. Such trends indicate that the decrease of film protection which accompanies an increase in pulsation frequency for a particular film injection hole cross-section geometry is not characterized by a single value of injectant Strouhal number as L/D is varied [2]. Instead, the decrease in film protection is dependent upon a number of characteristics, including the injectant Strouhal number, Str_c, the length-to-diameter ratio of the holes L/D, and the behavior of the film injectant as it passes through the holes. To obtain additional information on this last item, surveys of injectant velocity distributions are measured at the exit planes of injection holes.

4.3. Injectant velocity profiles at hole exits and injection behavior within the film holes

The velocity profiles at the exits of the film cooling holes are measured with an averaged injectant velocity of 5.0 m s^{-1} and no freestream flow (or external boundary layer) present. As mentioned earlier, the film cooling holes are inclined 35° from the plane of the test surface. Exits at the test surface extend over x/D from -0.9 to $+0.9$ and over z/D from -0.5 to $+0.5$. Velocity profile data for L/D of 1.6, 4.0 and 10.0 are presented in Fig. 8(a) as dependent upon x/D at $z/D = 0$. Velocity profile data for the same L/D are given in Fig. 8(b) as dependent upon z/D at $x/D = 0$.

The non-uniform velocity distribution could be present because of flow separation on the leeward side of the injection hole near its entrance from the plenum chamber, and the injectant velocity near the windward side of hole entrance is thus accelerated due to flow blockage from separation on the opposite side, whereas the flow just

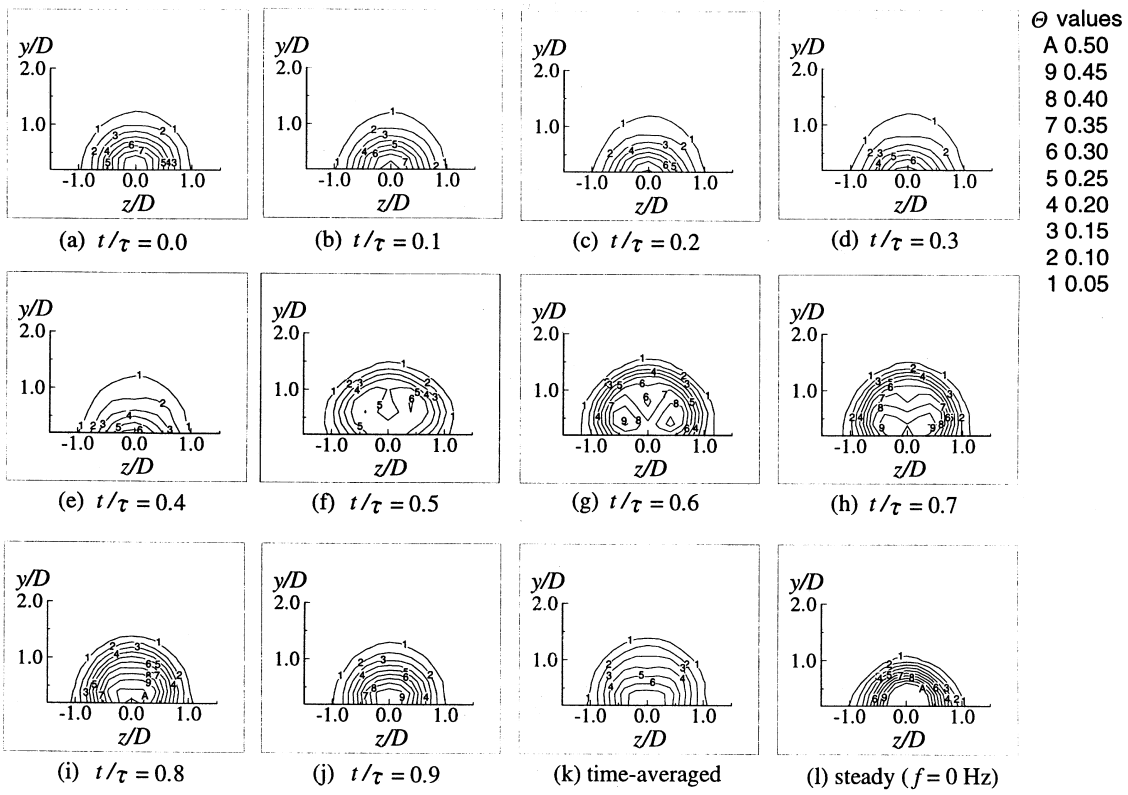

Fig. 5. Phase-averaged injectant concentration Θ distributions at $x/D = 5.0$ for $f = 32$ Hz and $L/D = 4$.

downstream of the separated flow is decelerated. However, non-uniformities in the injectant velocity profiles become smaller as the film advects through each hole because of turbulence diffusion.

Flow separation near the entrance of a $L/D = 3.5$ injection hole has been also described by Pietrzk et al. [13], and Leylek and Zerkle [14]. According to these investigators, high intensity turbulence would be generated because of the flow separation, which results in a highly non-uniform velocity profile, as well as a region of high turbulence intensity in the injectant at the hole exit. Such behavior is consistent with out $L/D = 4$ results in Fig. 8. The injectant velocity variations shown in Fig. 8, and the behavior of the injectant in the holes, both affect the performance of film cooling when subject to the influences of bulk flow pulsations. Higher injectant velocities near the windward edges of the smaller L/D holes cause the injectant to penetrate farther into the external boundary layer. The flow separations within the injectant holes are affected significantly by the pulsations [15, 16]. As L/D is smaller, the separation bubble formed at the hole entrance is nearer to the hole exit. Thus, the imposed pulsations of static pressure directly influence the size and character of the separation bubble, significantly altering the instantaneous injectant velocity distribution within and at the exits of the holes. It is consistent physically for the results in Figs. 4–7.

4.4. Adiabatic film cooling effectiveness distributions

Figure 9 shows local film cooling effectiveness variations in the streamwise direction downstream of and along the centerline of the central injection hole for $\bar{m} = 0.5$. Generally, this film cooling effectiveness decreases as pulsation frequency increases at each L/D and x/D, such decreases are more drastic when the injection hole length is shorter. In particular, the $L/D = 1.6$ centerline film effectiveness is remarkably reduced by $30 \sim 50\%$ at $f = 32$ Hz, as compared to the steady ($f = 0$ Hz) distribution. Differences between the 2 Hz to 16 Hz data at each L/D are generally small. Differences between pulsation and non-pulsation data thus generally become smaller as L/D increases from 1.6 to 4, and then from 4 to 10. When $L/D = 10$, changes to centerline film cooling effectiveness distributions from the bulk flow pulsations are then relatively minimal. When these data are com-

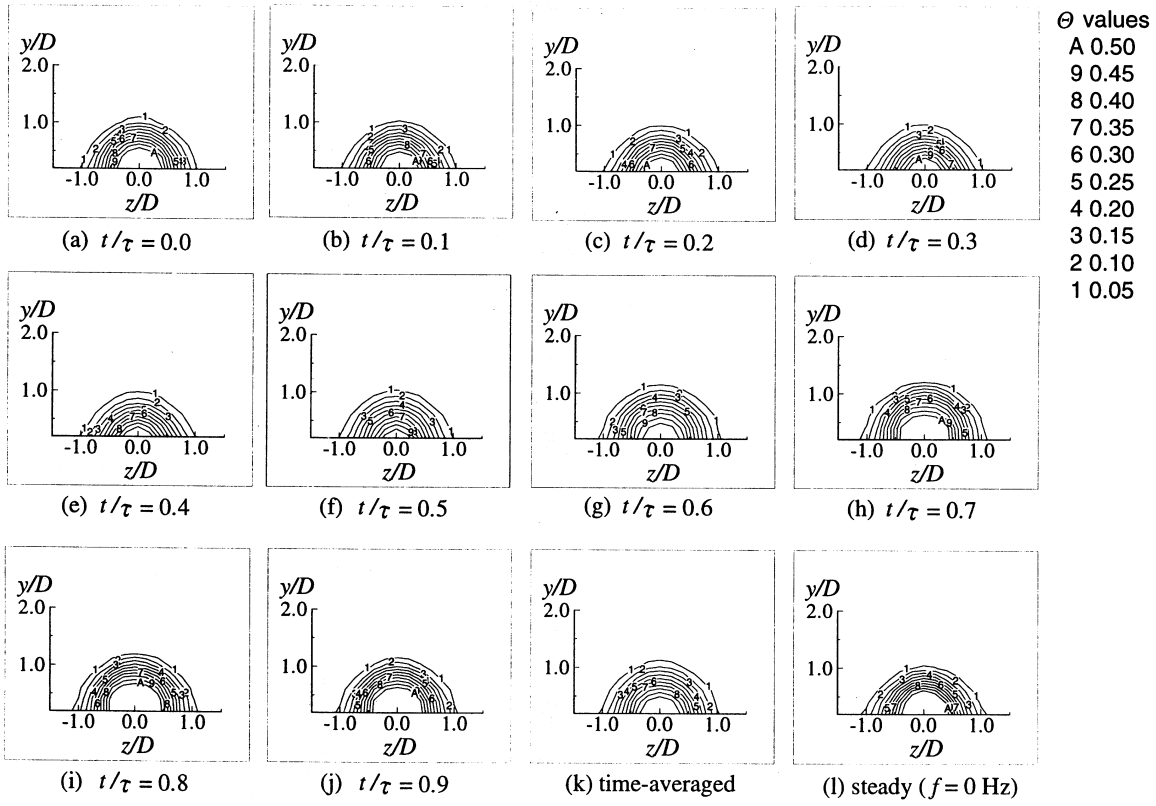

Fig. 6. Phase-averaged injectant concnetration Θ distributions at $x/D = 5.0$ for $f = 32$ hz and $L/D = 10$.

pared to results at other L/D, effectiveness values are higher at smaller x/D locations close to the holes as L/D increases. This is because of characteristics of injectant velocity profiles at hole exits such as the ones shown in Fig. 8.

Figure 10 shows spanwise-averaged film cooling effectiveness, η_m, determined from averages over z/D from -1.5 to 1.5. These values are smaller than the centerline effectiveness values, shown in the previous figure, because the region between the adjacent holes is not fully covered by the injectant. The data of Pedersen et al. [17] and Goldstein et al. [18], are compared to $L/D = 10$ results from the present study in Fig. 10(c), because their injection hole length produces fully developed velocity profiles at hole exits. The $f = 0$ Hz effectiveness values from the present study are somewhat larger than their results because their ratio of displacement thickness to the hole length is less, and their blowing ratio is slightly higher than present values. As a result, their injectant penetrates further into the freestream flow and the boundary layer, resulting in lower effectiveness values than the present results.

Considering the present spanwise-averaged results, the effects of the pulsations are largest in Fig. 10 at 32 Hz when $L/D = 1.6$. This is evident from spanwise-averaged effectiveness values with no pulsations, which are about 0.2 at $x/D = 10$. In contrast, values are only about 0.1 at the same location when 32 Hz pulsation are imposed, which gives a 100% effectiveness reduction. As the hole length increases, these reductions are less, until $L/D = 10$, when the influences of the pulsations on spanwise-averaged effectiveness are minimal.

4.5. Iso-energetic Stanton number ratio distributions

Centerline iso-energetic Stanton number ratios are presented in Fig. 11 for $\bar{m} = 0.5$. When compared at the same L/D and x/D, values generally increase with pulsation frequency for $L/D = 1.6$ and $L/D = 4$. As for the centerline effectiveness distributions, the largest variations with f occur for $L/D = 1.6$, whereas almost no change with pulsation frequency f are evident at each x/D in Fig. 11(c) for $L/D = 10$.

Spanwise-averaged iso-energetic Stanton number distributions in Fig. 12 *generally* increase with pulsation frequency when compared at the same L/D and x/D. These data thus show the trends which are qualitatively similar to the centerline values in the previous figure, except that increases relative to non-pulsation values are quantitatively less. In some cases, spanwise-averaged iso-

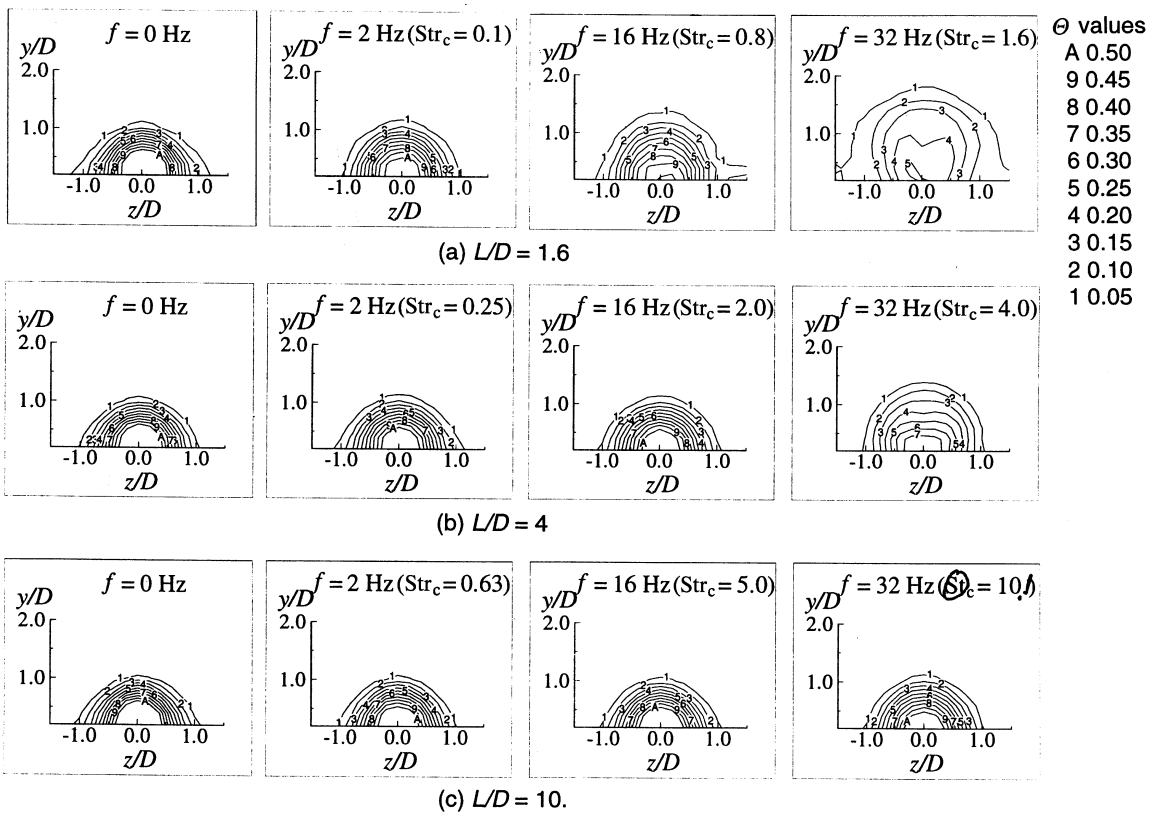

Fig. 7. Time-averaged injectant concentration Θ distributions at $x/D = 5.0$.

energetic Stanton number ratios decrease slightly as pulsation frequency increases. This is evident at $x/D > 10$ in Fig. 12(b) for $L/D = 4$, and at $x/D > 5$ in Fig. 12(c) for $L/D = 10$.

4.6. Overall film cooling performance parameter distributions

Spanwise-averaged magnitudes of overall film cooling performance parameters, $\dot{q}''/\dot{q}''_0$, are presented in Fig. 13 also for $\bar{m} = 0.5$. Values of $\dot{q}''/\dot{q}''_0$ are evaluated using procedures described by Ligrani and Lee [19, 20] using the spanwise-averaged effectiveness data in Fig. 10, the spanwise-averaged iso-energetic Stanton number ratio data in Fig. 12, and a Θ value of 1.67.

The largest $\dot{q}''/\dot{q}''_0$ variations with pulsation frequency (at each x/D value) are present for $L/D = 1.6$ in Fig. 13(a). In this case, the best overall film cooling protection (and the lowest $\dot{q}''/\dot{q}''_0$ distribution) are present when no pulsations are imposed. Protection then degrades continuously as the pulsation frequency increases. The effects of the pulsations are minimal in Fig. 13(c) for $L/D = 10.0$ since almost no $\dot{q}''/\dot{q}''_0$ changes with pulsation frequency are evident at each x/D.

Comparing data obtained using an imposed pulsation frequency of 32 Hz and different L/D in Fig. 13, shows increasing $\dot{q}''/\dot{q}''_0$ (and diminishing overall film cooling protection) at each x/D as L/D decreases. Similar qualitative trends are present at the other three pulsation frequencies investigated. At $f = 0$ Hz, $\dot{q}''/\dot{q}''_0$ again increases with decreasing L/D at each x/D, but the changes are quite small.

5. Summary and conclusions

The effects of injection hole length on film cooling from a single row of simple angle holes subject to bulk flow pulsations are investigated. Injection hole length to diameter ratios are 1.6, 4.0, and 10. Bulk flow pulsations of streamwise velocity and static pressure are imposed at frequencies of 2, 16, and 32 Hz. Corresponding injectant Strouhal numbers range from 0.1–10.1.

Time-averaged, phase-averaged, and steady (i.e. obtained with no pulsations) injectant distributions in the spanwise/normal plane at $x/D = 5$ show that greater alterations to injectant distributions occur as the hole length-to-diameter ratio decreases, and as the imposed

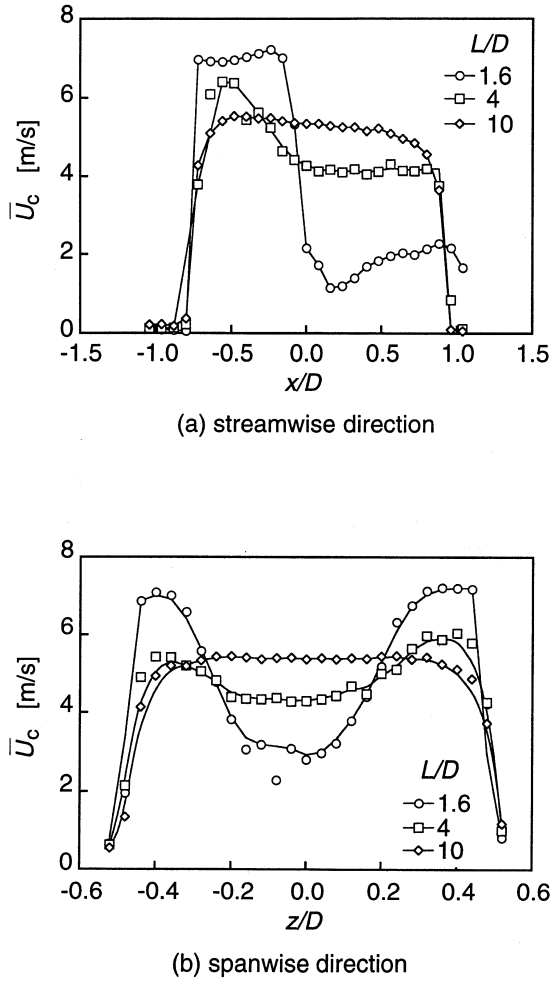

Fig. 8. Injectant time-averaged velocity profiles at the hole exit in the absence of freestream flow.

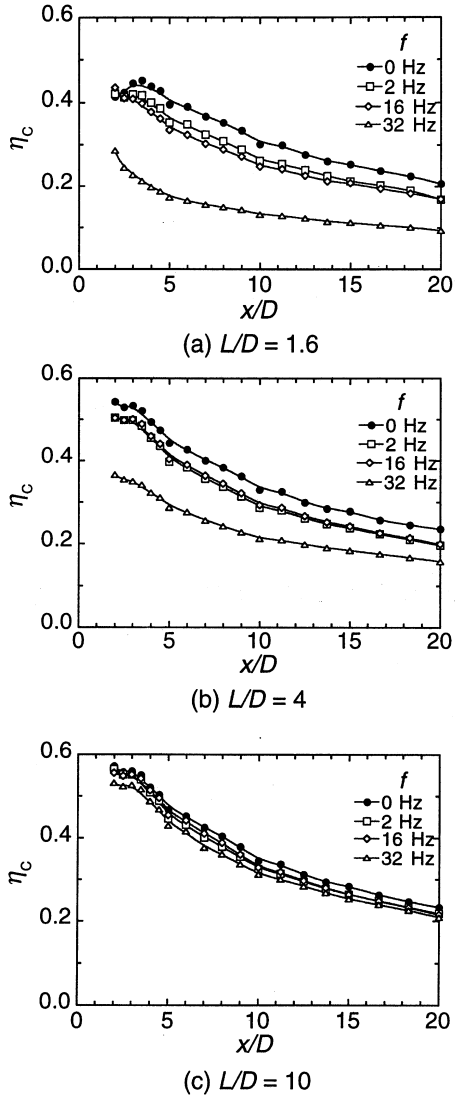

Fig. 9. Centerline adiabatic film cooling effectiveness for $\bar{m} = 0.5$.

pulsation frequency increases. The largest alterations occur using $L/D = 1.6$ holes subject to pulsations at 32 Hz, and are in the form of spreading of injectant concentrations over larger volumes compared to steady distributions. This results in diminished film cooling protection.

Phase-averaged injectant temperature distributions show periodic variations due to instantaneous changes to the injectant flow rate and due to instantaneous changes of the character of the injectant flow within the holes. The decrease in film protection is dependent upon a number of characteristics, including the injectant Strouhal number Str_c, the length-to-diameter ratio of the holes L/D, and the behavior of the film injectant as it passes through the holes.

When compared at particular x/D and L/D, centerline and spanwise-averaged adiabatic film cooling effectiveness magnitudes generally decrease, and centerline and spanwise-averaged iso-energetic Stanton number ratios generally increase, as the pulsation frequency increases. Changes are larger as the injection hole length is shorter and as the imposed pulsation frequency increases. As these alterations from the pulsations occur, the overall film cooling effectiveness parameter increases, which indicates decreased film cooling protection. These results are consistent with Ligrani et al. [3], who show decreases of film protection at similar experimental conditions at frequencies as low as 0.6 Hz and Str_c as low as 0.66. The present results show that when $L/D = 10$, little or not disruptions to the protection provided by the film at imposed pulsation frequencies ranging from 2 to 32

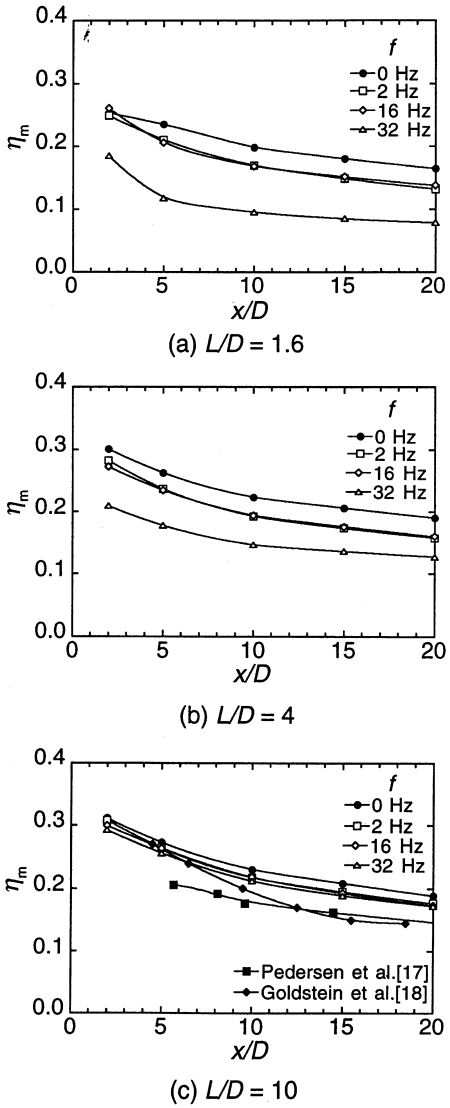

Fig. 10. Spanwise-averaged adiabatic film cooling effectiveness for $\bar{m} = 0.5$.

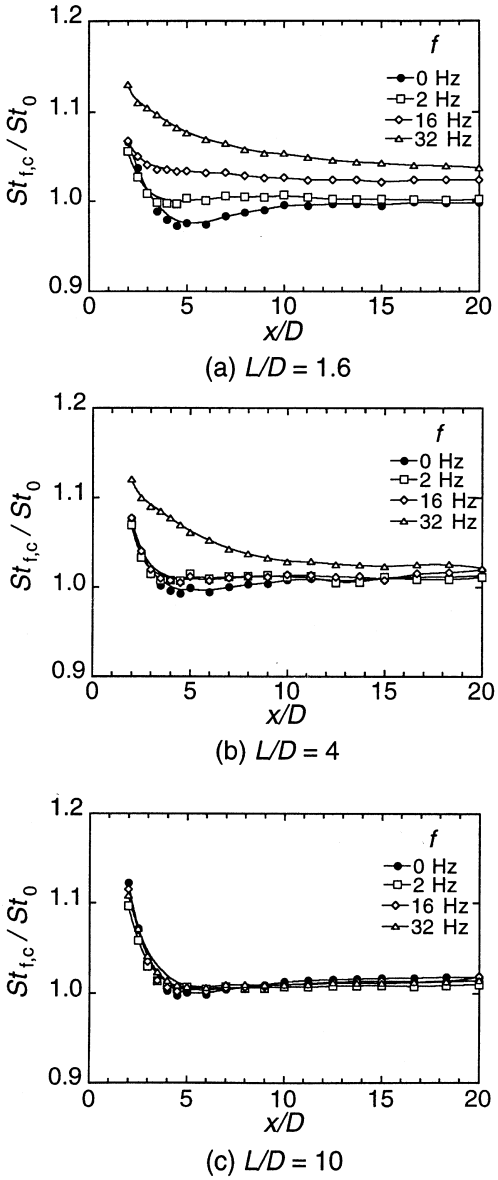

Fig. 11. Centerline iso-energetic Stanton number ratio for $\bar{m} = 0.5$.

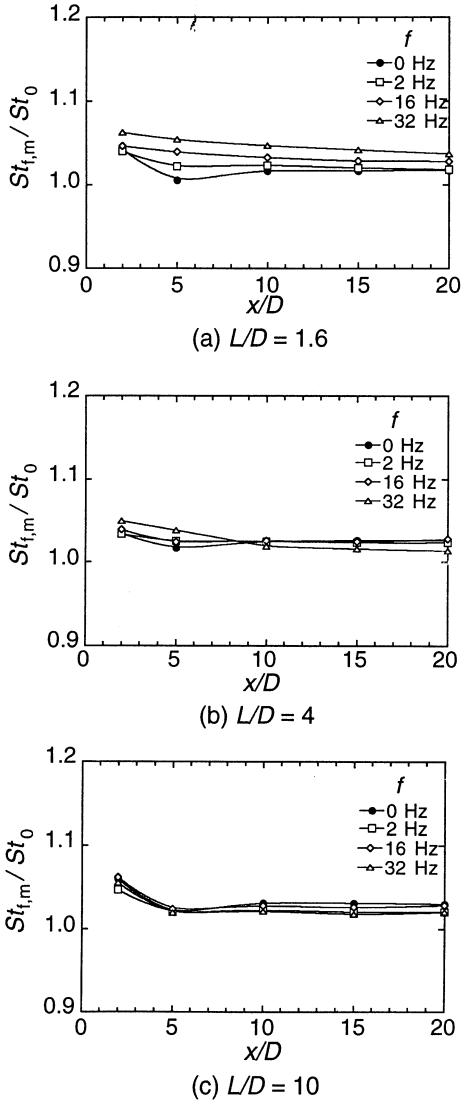

Fig. 12. Spanwise-averaged iso-energetic Stanton number ratio for $\bar{m} = 0.5$.

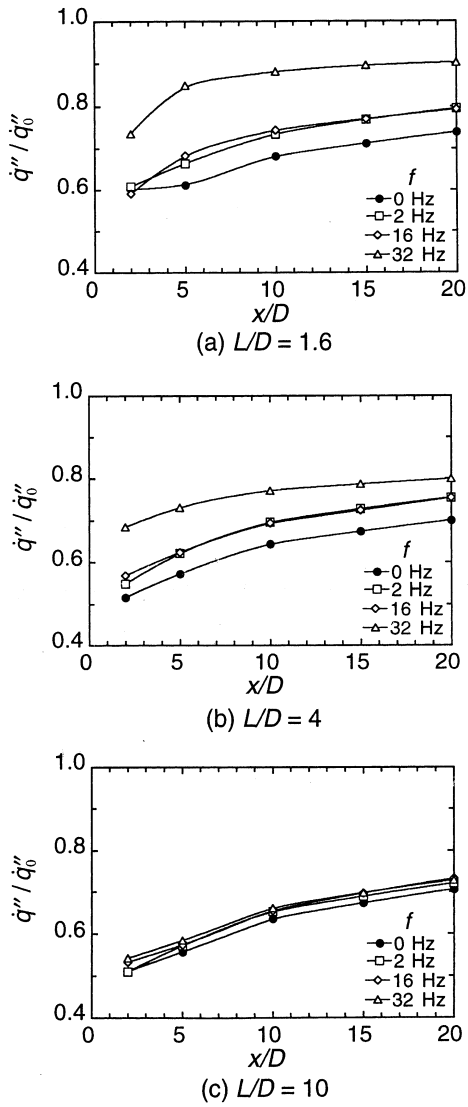

Fig. 13. Spanwise-averaged overall film cooling performance parameter for $\bar{m} = 0.5$.

Hz, which correspond to injectant Strouhal numbers from 0.63 to 10.0

Acknowledgement

The portions of this effort conducted at the University of Utah were sponsored by the National Science Foundation, Grant number CTS-9615196.

References

[1] Abhari RS, Epstein AH. An experimental study of film cooling in a rotating transonic turbine. ASME Journal of Turbomachinery 1994;116:63–70.

[2] Ligrani PM, Gong R, Cuthrell JM, Lee JS. Bulk flow pulsations and film cooling; Part 1: Injectant behavior. International Journal of Heat and Mass Transfer 1996;39:2271–82.

[3] Ligrani PM, Gong R, Cuthrell JM, Lee JS. Bulk flow pulsations and film cooling; Part 2: Flow structure and film effectiveness. International Journal of Heat and Mass Transfer 1996;39:2283–92.

[4] Abhari RS. Impact of rotor-stator interaction on turbine blade film cooling. ASME Journal of Turbomachinery 1996;118:103–13.

[5] Ligrani PM, Gong R, Cuthrell JM. Bulk flow pulsations and film cooling: flow structure just downstream of the holes. ASME Journal of Turbomachinery 1997, to appear.

[6] Ligrani PM, Gong R, Cuthrell JM, Lee JS. Effects of bulk

flow pulsations on film-cooled boundary layer structure. ASME Journal of Fluids Engineering 1997;119:56–66.
[7] Kline SJ, McClintock FA. Describing uncertainties in single sample experiments. Mechanical Engineering 1953;75:3–8.
[8] Al-Asmi K, Castro IP. Production of oscillatory flow in wind tunnels. Experiments in Fluids 1993;15:33–41.
[9] Karlsson SK. An unsteady turbulent boundary layer. Journal of Fluid Mechanics 1959;14:622–36.
[10] Doorly DJ, Oldfield MLJ. Simulation of the effects of shock wave passing on a turbine rotor blade. ASME Journal of Engineering Gas Turbines and Power 1985;107:998–1006.
[11] Ligrani PM, Williams WW. Effects of an embedded vortex on injectant from a single film-cooling hole in a turbulent boundary layer. ASME Journal of Turbomachinery 1990;112:428–36.
[12] Ligrani PM, Wigle JM, Ciriello S, Jackson SW. Film-cooling from holes with compound angle orientations: Part 1—Results downstream of two staggered rows of holes with 3d spanwise spacing. ASME Journal of Heat Transfer 1994;116:341–52.
[13] Pietrzyk JR, Bogard DG, Crawford ME. Hydrodynamic measurements of jets in crossflow for gas turbine film cooling applications. ASME Journal of Turbomachinery 1989;111:139–45.
[14] Leylek JH, Zerkle RD. Discrete-jet film cooling: a comparison of computational results with experiments. ASME Journal of Turbomachinery 1994;116:358–68.
[15] Miller JA, Pucci PF. Heat transfer to an airfoil in oscillating flow. ASME Journal of Engineering for Power 1971;October:461–8.
[16] Krause E, Schweitzer WB. The effect of an oscillatory free-stream-flow on a NACA-4412 profile at large relative amplitudes and low Reynolds-numbers. Experiments in Fluids 1990;9:159–66.
[17] Pedersen DR, Eckert ERG, Goldstein RJ. Film cooling with large density differences between the mainstream and the secondary fluid measured by the heat-mass transfer analogy. ASME Journal of Heat Transfer 1977;99:620–7.
[18] Goldstein RJ, Yoshida T. The influence of a laminar boundary layer and laminar injection on film cooling performance. ASME Journal of Heat Transfer 1982;104:355–62.
[19] Ligrani PM, Lee JS. Film cooling from two staggered rows of compound angle holes at high blowing ratios. International Journal of Rotating Machinery 1996;2:201–8.
[20] Ligrani PM, Lee JS. Film cooling from a single row of compound angle holes at high blowing ratios. International Journal of Rotating Machinery 1996;2:259–67.